electronics

MDPI

Article

Research on an Algorithm for High-Speed Train Positioning and Speed Measurement Based on Orthogonal Time Frequency Space Modulation and Integrated Sensing and Communication

Jianli Xie [1,*], Yong Hao [1], Cuiran Li [1] and Huiqin Wang [2]

[1] School of Electronics and Information Engineering, Lanzhou Jiaotong University, Lanzhou 730070, China; 12221829@stu.lzjtu.edu.cn (Y.H.); licr@mail.lzjtu.cn (C.L.)
[2] School of Computer and Communication, Lanzhou University of Technology, Lanzhou 730050, China; whq1222@lut.edu.cn
* Correspondence: xiejl@mail.lzjtu.cn

Abstract: The Doppler effect caused by the rapid movement of high-speed rail services has a great impact on the accuracy of train positioning and speed measurement. Existing train positioning algorithms require a large number of trackside equipment and sensors, resulting in high construction and maintenance costs. Aiming to solve the above two problems, this article proposes a train positioning algorithm based on orthogonal time–frequency space (OTFS) modulation and integrated sensing and communication (ISAC). Firstly, based on the OTFS, the positioning and speed measurement architecture of communication awareness integration is constructed. Secondly, a two-stage estimation (TSE) algorithm is proposed to estimate the delay Doppler parameters of HST. In the first stage, a low-complexity coarse grid search is used, and in the second stage, a refined off-grid search is used to obtain the delay Doppler parameters. Then, the time difference of arrival/frequency difference of arrival (TDOA/FDOA) algorithm based on multiple base stations is used to locate the target, the weighted least square method is used to calculate the location, and the Cramér–Rao lower bound (CRLB) for positioning and speed measurement is derived. The simulation results demonstrate that, compared to GNSS/INS and OFDM radars, the algorithm exhibits enhanced positioning and speed measurement accuracy.

Keywords: OTFS; ISAC; parameter estimation; time difference of arrival; high-speed rail communication

check for updates

Citation: Xie, J.; Hao, Y.; Li, C.; Wang, H. Research on an Algorithm for High-Speed Train Positioning and Speed Measurement Based on Orthogonal Time Frequency Space Modulation and Integrated Sensing and Communication. *Electronics* **2024**, *13*, 4397. https://doi.org/10.3390/electronics13224397

Academic Editors: Muhammad Usman Hadi and Muhammad Ikram Ashraf

Received: 8 October 2024
Revised: 7 November 2024
Accepted: 8 November 2024
Published: 9 November 2024

Copyright: © 2024 by the authors. Licensee MDPI, Basel, Switzerland. This article is an open access article distributed under the terms and conditions of the Creative Commons Attribution (CC BY) license (https://creativecommons.org/licenses/by/4.0/).

1. Introduction

Train positioning technology plays a crucial role in ensuring the efficiency and safety of railway operations. Train positioning technology based on a single measurement method, such as track circuit positioning, odometer positioning, radar speed measurement positioning, etc., cannot meet the requirements of the positioning accuracy and the positioning continuity [1].

The current mainstream method for train positioning is combination positioning technology, among which the global navigation satellite system (GNSS) and inertial navigation system (INS) can provide accurate position information for trains. However, when a train passes through environments such as bridges, mountains and tunnels, the complex and changeable railway environment along the line can easily interfere with the transmission of GNSS signals, leading to a decline in positioning performance [2]. An inertial navigation system is an autonomous navigation system. Although it has a strong anti-interference ability, it is limited by the characteristics of its own micro inertial devices, and its position and attitude error information gradually accumulates, making it difficult to provide long-term accurate positioning information [3].

In the high-speed train (HST) positioning and speed measurement system, millimeter wave radar and light detection and ranging (LIDAR) can work in various environments,

because they are not affected by light and weather conditions [4]. However, the construction and maintenance costs of high-precision radar systems and related equipment are high, requiring regular maintenance and calibration. Therefore, utilizing existing trackside base stations of the railway communication system to achieve low-cost and high-precision HST positioning and speed measurement is an unresolved problem.

Integrated sensing and communication (ISAC) is a new type of information processing technology that integrates communication and sensing functions into the same system, offering significant advantages in terms of equipment cost and size, system performance and spectrum utilization [5]. ISAC breaks the working mode of traditional communication or positioning systems, achieving both high-quality communication and high-precision positioning in one system [6]. In the HST scenarios, the ISAC modules can be added to the existing trackside base stations to realize the high-precision train positioning function. Compared with the current mainstream train positioning method, the ISAC-based positioning and speed measurement method has the following advantages: ISAC allows the communication and perception subsystems to share the same hardware, while realizing different functions, so it does not need to install additional sensors beside the track. Using the existing base station for reconstruction can realize the train positioning function and reduce the construction and maintenance costs. In the research on target sensing using ISAC systems, many studies have proposed corresponding solutions to improve the accuracy of target state sensing. In [7], the radial velocity of vehicle motion is obtained by using the echo signal reflected from the vehicle through a matched filter and the tracking error of the vehicle is minimized by using an extended Kalman filter (EKF). In [8], a novel and flexible orthogonal frequency division multiplexing (OFDM)-based sensing framework is developed, where the range-Doppler maps (RDMs) obtained using the cyclic cross-correlation (CCC) algorithm provide better sensing performance than the RDMs obtained based on the conventional point-by-point segmentation in the low-signal-to-noise ratio (SNR) region. In [9], to improve the accuracy of vehicle state sensing, a novel joint solution algorithm is proposed, which utilizes the structural features of the channel model, such as random channel fading, multipath propagation interference and the Doppler effect, and then employs downlink multicarrier signal echo sensing to derive the vehicle position and channel state and jointly estimate the vehicle speed.

With the gradual maturity of ISAC technology based on multicarrier waveforms, the application of the orthogonal time–frequency space (OTFS) modulation technique has attracted extensive attention from scholars. The core idea of OTFS is to use transforms to characterize the time–frequency bi-selective channels in the delay Doppler (DD) domain, so as to obtain a sparse channel that maintains good communication performance in high-mobility scenarios [10]. The OFDM is widely used in current wireless communication systems; the orthogonality between subcarriers is destroyed due to serious Doppler effect, which also makes OFDM modulation unable to carry out efficient and reliable communication in high-speed mobile environments [11]. The OTFS is more suitable than OFDM for communication transmission in high-speed mobility environments.

Research on OTFS-ISAC is currently on the rise [12]. OTFS is characterized by mapping data symbols and pilots into a DD domain grid in a specific way, where the size of the DD grid depends on the available bandwidth and signal duration, which is consistent with the concept of fast and slow time in radar signal processing [13,14]. By sensing the multipath delay and Doppler parameters of the target in the DD domain, the corresponding target distance and velocity can also be directly obtained. Therefore, the integration of OTFS and ISAC has been widely investigated.

In [15], regarding the theoretical performance indicators that OTFS-ISAC can achieve, the authors evaluate the effectiveness of OTFS modulation for ISAC transmission, proving that OTFS can maintain the same range and velocity estimation accuracy as frequency modular continuous wave (FMCW) radar. In [16], a scheme based on the maximum likelihood (ML) function is proposed in the OTFS-ISAC system based on multiple-input multiple-output (MIMO), which performs joint target detection and parameter estimation in

discovery mode and high-resolution parameter estimation in tracking mode. Numerical results show that the proposed method can reliably detect multiple targets while approaching the Cramér–Rao lower bound (CRLB) of the corresponding parameter estimation problem.

Some studies consider the application of OTFS-ISAC in multi-base-station regimes but do not take into account HST application scenarios. Reference [17] discusses the problem of three-dimensional positioning of a single target in an ISAC system. Firstly, a joint position estimation model of direction of arrival (DOA) and time difference of arrival (TDOA) is established, and then an efficient two-step weighted least squares (TWLS) solution is derived. When the measurement error is large, the TWLS solution will reduce the positioning accuracy. Reference [18] proposes an integrated design approach in the delay Doppler domain, bypassing the time–frequency dimension, and significantly reduces the time–frequency resources required by the radar through a multi-station collaborative radar architecture. Reference [19] starts with the modulation principle of OTFS and delves deeper, layer by layer, to analyze the OTFS-ISAC system architecture under two different radar modes: monostatic radar and bistatic radar. It briefly discusses the communication and perception performance of OTFS-ISAC relative to OFDM. Reference [20] proposed a novel Doppler positioning scheme in HST scenarios, which arranges access points (APs) connected to base stations on the trackside and utilizes fractional Doppler estimation in OTFS to achieve higher positioning and velocity estimation accuracy, with lower requirements for bandwidth and hardware.

Based on the above analysis, this article proposes an HST positioning and velocity measurement algorithm based on OTFS-ISAC. The main contributions of this article are as follows:

1. Different from the existing high-speed train positioning and speed measurement methods, this paper proposes a communication perception integrated positioning model based on OTFS. The proposed algorithm does not require the deployment of additional trackside sensors and can achieve stable positioning and speed measurement of high-speed trains using only existing trackside base stations.
2. In order to improve the accuracy of target parameter estimation, a two-stage parameter estimation (TSE) algorithm is proposed, which uses the propagation characteristics of the DD domain to estimate parameters in the grid, and can accurately estimate the Doppler and delay parameters of high-speed trains.
3. Through the cooperation of multiple base stations, the information of TDOA and frequency difference of arrival (FDOA) are used, and then weighted least squares (WLS) methods are used to locate and measure the speed of high-speed trains.

The rest of this article is organized as follows: The communication-sensing integrated positioning model based on OTFS is designed in Section 2. Section 3 proposes the two-stage estimation (TSE) algorithm, which utilizes the propagation characteristics of the DD domain to accurately estimate the Doppler and time-delay parameters of the targets in the grid. In Section 4, multiple base stations collaborate to utilize TDOA and FDOA information and then use WLS for positioning and speed measurement of HSTs. We complete the simulation comparison experiment in Section 5. Finally, the conclusion of this article is presented in Section 6.

2. Train Positioning Model Based on OTFS-ISAC

2.1. Scene Modeling

Consider the OTFS-ISAC positioning scenario shown in Figure 1, where three base stations are located next to the railroad and equipped with integrated sensing modules for transmitting and receiving OTFS-ISAC signals. The HST, as the sensing target and the communication receiver, is equipped with a receiver on the roof to receive and demodulate the downlink communication signals sent by the base stations. The antenna arrays of the base stations are arranged in parallel with the running line of the HST, but the position and speed information of the HST are unknown. The base station has two functions: one is to communicate with the communication receiver, and the other is to accomplish the

target speed measurement and distance measurement. When the HST moves forward at the speed of v, the base station transmits OTFS-ISAC signals, the communication receiver on the roof demodulates the received signals and obtains the communication signals, and at the same time, the HST reflects the integrated signals as a target, so that the reflected echo signals are received by the base station [21]. The integrated sensing module in the base station first uses a two-stage parameter estimation algorithm to estimate the parameters of the target and obtain the delay and Doppler parameters, and then uses TDOA/FDOA to locate and measure the speed of the target.

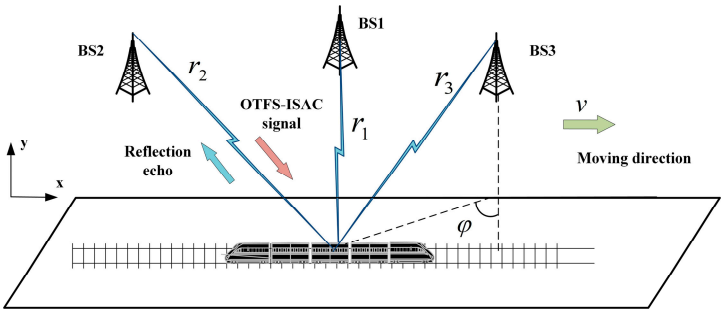


Figure 1. Schematic diagram of OTFS-ISAC positioning and speed measurement in the HST scenario.

2.2. Design of ISAC Signal Based on OTFS

As shown in Figure 2, the OTFS- ISAC transceiver adopts a configuration similar to that of a monostatic radar, consisting of an integrated transmitter and receiver. The system senses the target and estimates relevant parameters while communicating with the target. That is, the OTFS sensing integrated signal generated by the transmitter can achieve dual functions of transmission and perception simultaneously. For communication, the OTFS-ISAC transceiver can communicate bidirectionally with the user or the receiver at the target end. In terms of sensing, the active downlink sensing method is adopted. The integrated signal sent by the transmitter is reflected by the target, and the receiver processes the echo signal to complete the detection of target perception. After receiving the echo signal $r_R(t)$, it needs to be restored to the DD domain for speed and distance parameter estimation of the target.

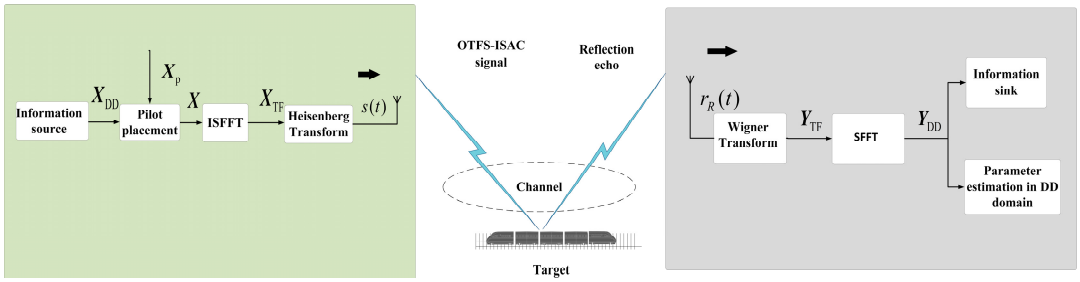


Figure 2. Block diagram of OTFS-ISAC system.

2.2.1. Transmitter

At the communication transmitter, the transmit modulation symbol vector $x \in \mathbb{C}^{1\times MN}$ of length MN is placed in the two-dimensional plane of the DD domain and arranged into a two-dimensional matrix X_{DD}, where N and M represent the number of OTFS symbols and the number of subcarriers, respectively. The $X_{\mathrm{DD}}[l,k] \in X_{\mathrm{DD}}$ represents the transmission modulation signal at the grid index of the k_{th} Doppler domain and the l_{th} delay domain in the two-dimensional plane grid of the delay Doppler domain. k and l are the Doppler and time delay grid indices for $l = 0, 1, \cdots, M-1, k = 0, 1, \cdots, N-1$. Therefore, X_{DD} is called the transmit modulation symbol matrix of the DD domain. In this article, we consider the superimposed frequency pilot scheme, in which the frequency pilot symbols

X_{p} are superimposed on X_{DD} in the delay Doppler domain, that is, $X = X_{\mathrm{DD}} + X_{\mathrm{p}}$, where the arrangement of the frequency pilot symbols can be expressed as

$$X_{\mathrm{p}}[l,k] = \begin{cases} \sqrt{MN\sigma_p^2}, \ (l,k) = (l_p, k_p) \\ 0, \ others \end{cases} \tag{1}$$

where $0 \leq l_p \leq M-1$ and $0 \leq k_p \leq N-1$ denote the position of the frequency pilot symbol in the delay Doppler domain, and the average energy of the frequency pilot symbols can be defined as

$$E\left\{ \left| X_p[l,k] \right|^2 \right\} = \sigma_p^2 \tag{2}$$

The OTFS pilot design is shown in Figure 3, where data symbols are arranged on the entire delay Doppler plane, and non-zero pilot symbols are only placed in one delay Doppler grid (l_p, k_p), which is superimposed onto the data symbol $X_{\mathrm{DD}}[l_p, k_p]$. Zero-padding is performed for pilots at other delay Doppler grids. Compared with the scheme of arranging protection areas around the embedded pilot (EP) [22], there is no dedicated grid for the pilot arrangement in the superimposed pilot scheme, which can reduce pilot overhead and improve spectral efficiency.

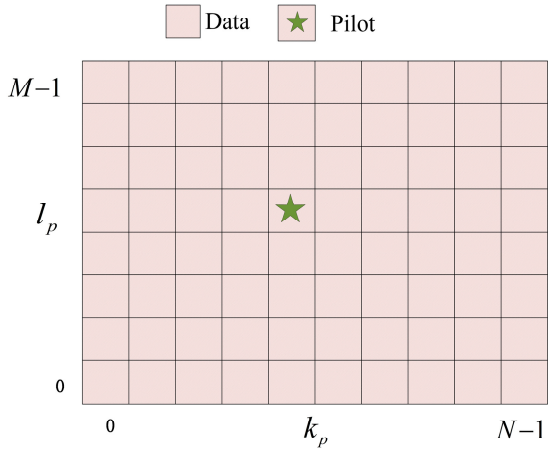


Figure 3. Delay Doppler domain frequency guidance design.

Then, the transmitter processes X and maps it to the time domain in two steps. In the first step, $X_{\mathrm{TF}}[n,m]$ is mapped to the time–frequency domain using the inverse symplectic finite Fourier transform (ISFFT), as

$$X_{\mathrm{TF}}[n,m] = \frac{1}{\sqrt{NM}} \sum_{k=0}^{N-1} \sum_{l=0}^{M-1} X_{DD}[k,l] e^{j2\pi\left(\frac{nk}{N} - \frac{ml}{M}\right)} \tag{3}$$

where $m = 0, 1, \cdots, M-1$, $n = 0, 1, \cdots, N-1$ denote the frequency and time grid indexes, respectively. In the second step, the time-domain baseband signal of OTFS-ISAC can be obtained using the Heisenberg transform, as

$$s(t) = \sum_{n=0}^{N-1} \sum_{m=0}^{M-1} X_{\mathrm{TF}}[n,m] g_{tx}(t - nT) e^{j2\pi m\Delta f(t-nT)} \tag{4}$$

where k and l are the Doppler and time delay grid indices, m and n are the frequency and time grid indices, the duration of each OTFS symbol is set to T, the carrier spacing is set to Δf, and g_{tx} represents the pulse shaping filter at the transmitter. After the baseband signal is upconverted, the OTFS-ISAC signal is sent through the transmit antenna.

2.2.2. Receiver

The transmitter generates and transmits the OTFS signal; the receiver on the roof of the HST receives the communication signal and demodulates it, while the receiver at the base station receives the echo signal reflected by the target and extracts the target parameter information. In the integrated communication and perception scenario, radar sensing typically operates in high-frequency bands such as sub-6 GHz and terahertz bands, which are dominated by line-of-sight transmission. Therefore, the channel between the base station transmitter and the target is considered to be a single direct channel. This article considers a time-delay Doppler channel with perception targets (or paths), as

$$h(\tau,\mu)=\sum_{i=1}^{P}h_i\delta(\tau-\tau_i)\delta(\mu-\mu_i) \tag{5}$$

where τ_i and μ_i are the delay and Doppler parameters of the i_{th} target, h_i represents the complex channel gain, and $\delta(\cdot)$ represents the Dirichlet function. After the transmitted OTFS signal passes through the DD domain radar channel, the received echo signal $r_R(t)$ at the receiver can be expressed as

$$r_R(t)=\iint h_R(\tau,\mu)s(t-\tau)e^{j2\pi\mu(t-\tau)}d\tau d\mu+\omega(t) \tag{6}$$

where $h_R(\tau,\mu)=h(\tau,\mu)e^{j2\pi f_c\tau}$ represents the equivalent DD domain radar sensing channel, and $\omega(t)$ represents additive Gaussian white noise. After the received signal $r(t)$ undergoes analog-to-digital (A/D) and serial–parallel conversion, the time-domain baseband received signal is obtained, that is, $r(t)=r_R(t)e^{-j2\pi f_c t}$; the specific expression is shown in (7).

$$r(t)=\iint h(\tau,\mu)s(t-\tau)\mathrm{e}^{j2\pi\mu t}d\tau d\mu \tag{7}$$

Then, OTFS demodulation is performed on the $r(t)$. Firstly, the Wigner transform is used to enter the time–frequency (TF) domain to obtain the received modulation symbol matrix $Y_{\mathrm{TF}}\in\mathbb{C}^{M\times N}$, which is expressed as

$$Y_{\mathrm{TF}}[n,m]=\int_{\infty}^{\infty}r(t)g_{rx}(t-nT)e^{-j2\pi m\Delta f(t-nT)} \tag{8}$$

where g_{rx} stands for the receiver pulse shaping filter. Then, the received signal in the TF domain is transformed into DD domain through the symplectic finite Fourier transform (SFFT), as

$$Y_{\mathrm{DD}}[k,l]=\frac{1}{\sqrt{MN}}\sum_{n=0}^{N-1}\sum_{m=0}^{M-1}Y_{\mathrm{TF}}[n,m]e^{-j2\pi(\frac{nk}{N}-\frac{ml}{M})} \tag{9}$$

where $Y_{\mathrm{DD}}[k,l]\in Y_{\mathrm{DD}}$ denotes the received modulation signal in the k_{th} Doppler domain and l_{th} time-delay domain at the grid index on the DD domain. So far, the transformation of the received signal from the TF domain to the DD domain has been completed.

3. Target Parameter Estimation

Traditional radar signal processing algorithms often perform parameter estimation in the time–frequency domain, while OTFS radar can process signals in the DD domain and directly obtain the target's moving velocity by obtaining the target's Doppler frequency shift information [23]. This feature can be used to search on a two-dimensional (2D) grid in the DD domain, gradually narrowing down the area containing the true values of Doppler and delay parameters. In this section, the TSE algorithm is used to estimate the parameters of the target. In the first stage, a uniform grid is used for search to obtain rough estimates. Then, we continue off-grid search in the area established in the first stage. The proposed TSE algorithm process is described below.

At the first stage, in order to reduce the uncertainty area, a grid parameter search is performed on the discrete grid of the delay Doppler plane, as

$$\Lambda_i = \left\{ \left(\frac{l}{M\Delta f}, \frac{k}{NT} \right), l = 0 \ldots, M-1, k = -\frac{N}{2}, \ldots, \frac{N}{2} - 1 \right\} \tag{10}$$

When the values of delay and Doppler are integer multiples of the delay resolution and Doppler resolution, $\tau_i = \frac{l_i}{M\Delta f}$, $\mu_i = \frac{k_i}{NT}$, the received signal $Y[l,k]$ in the time-delay Doppler domain can be approximated as a two-dimensional circular shift in the transmitted signal [24], as

$$Y[l,k] \approx \sum_{i=1}^{P} e^{j2\pi(\frac{l-l_i}{M})\frac{k_i}{N}} \alpha_i(l,k) X[[l-l_i]_M, [k-k_i]_N] + \widetilde{W}[l,k] \tag{11}$$

where $\alpha_i(l,k) = \begin{cases} 1 & l_i \le l \le M \\ \frac{N-1}{N} e^{-j2\pi(\frac{[k-k_i]_N}{N})} & 0 \le l \le l_i \end{cases}$ represents the linear phase shift in the Doppler domain caused by the cyclic displacement of time-domain samples. $\widetilde{W}[l,k]$ denotes the noise. Then, the maximum estimate obtained is

$$(\hat{l}_i, \hat{k}_i) = \underset{(\hat{l}_i, \hat{k}_i) \in \Lambda}{\operatorname{argmax}} \left| (\Gamma_i x)^H \left(y - \sum_{j=1}^{i-1} \Gamma_j x(\hat{\tau}_j, \hat{\mu}_j) \right) \right|^2 \tag{12}$$

where $\Gamma_i x$ represents the useful signal and $\Gamma_j x$ represents the interfering signal. By using this formula, the index of time delay Doppler in the grid can be obtained. At this point, the estimated time delay $\hat{\tau}_i$ is set between $\frac{\hat{l}_i - 1}{M\Delta f}$ and $\frac{\hat{l}_i + 1}{M\Delta f}$; the estimated Doppler $\hat{\mu}_i$ is set between $\frac{\hat{k}_i - 1}{NT}$ and $\frac{\hat{k}_i + 1}{NT}$. Therefore, the lower limit and upper limit of the uncertainty area are determined. The search area of the second stage is

$$\Lambda_i = \left\{ (\tau, \mu), \frac{\hat{l}_i - 1}{M\Delta f} \le \tau \le \frac{\hat{l}_i + 1}{M\Delta f}, \frac{\hat{k}_i - 1}{NT} \le \mu \le \frac{\hat{k}_i + 1}{NT} \right\} \tag{13}$$

At the second stage, it is necessary to perform an off-grid search on the region Λ_i established in the first stage and solve the two-dimensional maximization problem in (14)

$$(\hat{\tau}_i, \hat{\mu}_i) = \arg \max_{(\tau_i, \mu_i) \in \Lambda_i} \left| (\Gamma_i x)^{\mathrm{H}} y_i \right|^2 \tag{14}$$

where $y_i = y - \sum_{j=1}^{i-1} \Gamma_j x(\hat{\tau}_j, \hat{\mu}_j)$; the meaning is to subtract the interference term $\Gamma_j x$ from the received signal y. Using the golden section, which belongs to the interval shrinkage method, the interval containing the best Doppler and delay solutions is gradually shrunk until the length of the interval is zero, and the shrinkage ratio $\rho \in [0,1]$ is set to $\frac{\sqrt{5}-1}{2}$. Based on the estimated delay and Doppler, the target distance and velocity can be calculated as $\hat{d}_i = \frac{\hat{\tau}_i c}{2}$ and $\hat{v}_i = \frac{\hat{\mu}_i c}{2 f_c}$.

When estimating the azimuth information in the angular domain, the maximum likelihood estimation algorithm is utilized to estimate the angular domain information [25], as

$$\hat{\varphi} = \underset{\varphi}{\operatorname{argmax}}\ p(\mathrm{r}_R(t) | \varphi) \tag{15}$$

where φ represents the included angle between the connecting line between the base station and HST and the relative movement velocity v_0. After completing the parameter estimation using the two-stage parameter estimation algorithm, the Doppler and delay

values of the HST can be obtained by each base station, respectively, which are converted into TDOA/FDOA information after differentiation and are processed for the localization and velocimetry solving in the next chapter.

The proposed two-stage parameter estimation algorithm is shown in Algorithm 1.

Algorithm 1: Proposed two-stage parameter estimation algorithm.

Input: Received vector y, transmit vector x.
Output: Estimated time-delay Doppler parameters $(\hat{\tau}, \hat{\mu})$.
1: Initialization: $y_i = y - \sum_{j=1}^{i-1} \Gamma_j x(\hat{\tau}_j, \hat{\mu}_j)$, $\rho = \frac{\sqrt{5}-1}{2}$;
2: **for** $i = 1 : P$ **do**
3: Calculating (12) yields the time-delay Doppler index $(\hat{l}_i, \hat{k}_i)$;
4: $a_u = \frac{\hat{l}_i - 1}{M\Delta f}$, $a_l = \frac{\hat{l}_i + 1}{M\Delta f}$, $b_u = \frac{\hat{k}_i + 1}{NT}$, $b_l = \frac{\hat{k}_i - 1}{NT}$;
5: **repeat**
6: $I_a = a_u - a_l$, $I_b = b_u - b_l$;
7: $a_1 = a_l + (1-\rho) I_a$, $a_2 = a_l + \rho I_a$;
8: $b_1 = b_l + (1-\rho) I_b$, $b_2 = b_u + \rho I_b$;
9: $f_{11} = \left| (\Gamma_i(a_1, b_1)x)^H y_i \right|^2$, $f_{12} = \left| (\Gamma_i(a_1, b_2)x)^H y_i \right|^2$;
10: $f_{21} = \left| (\Gamma_i(a_2, b_1)x)^H y_i \right|^2$, $f_{22} = \left| (\Gamma_i(a_2, b_2)x)^H y_i \right|^2$;
11: **switch** $\max\{f_{11}, f_{12}, f_{21}, f_{22}\}$ **do**
12: **case1** f_{11}, $a_u = a_2$, $b_u = b_2$;
13: **case2** f_{12}, $a_u = a_2$, $b_l = b_1$;
14: **case3** f_{21}, $a_l = a_1$, $b_u = b_2$;
15: **case4** f_{22}, $a_l = a_1$, $b_l = b_1$;
16: **end**
17: **until** Stopping criteria: $\hat{\tau}_i = \frac{a_l + a_u}{2}$, $\hat{\mu}_i = \frac{b_l + b_u}{2}$;
18: **end**

4. Radar Positioning and Speed Measurement

In general, the process of mobile target localization can be roughly divided into two steps. The first step is to obtain measurement information for position estimation. Secondly, based on the measurement information, the positioning algorithms are used to estimate the position and velocity of the target. Due to the less strict synchronization requirements between transceivers, TDOA/FDOA is often used as measurement information for positioning. The most common method in TDOA/FDOA positioning and solving algorithms is WLS, which has the characteristics of easy implementation and high computational efficiency. Therefore, the WLS method is selected in this article for positioning and speed measurement calculation.

4.1. Positioning Method Based on TDOA/FDOA

TDOA and FDOA are two common positioning methods that calculate the distance and velocity between the nodes by measuring the arrival time difference and frequency difference of signals, thus achieving positioning and speed measurement. There are three types of TDOA/FDOA positioning scenarios: (1) fixed base station to mobile target; (2) mobile base station to fixed target; (3) mobile base station to mobile target. These positioning scenarios all utilize the measured FDOA information and the position and velocity information between the base stations to form a nonlinear equation system, and then obtain the position and velocity information of the target by solving the equation system. For FDOA positioning, Doppler shift can be described as

$$\mu = \frac{f_0}{c} v_0 \cos \varphi \tag{16}$$

where v_0 is the relative velocity between the target and the base station; f_0 is the frequency of the transmitted signal.

This article considers a 2D localization and speed measurement scenario with an HST as the target, assuming that there are three fixed base stations with known positions and one target, one of which serves as a reference base station. The position and velocity vectors of the target to be estimated are $p = [x, y]^{\mathrm{T}}$ and $u = [\dot{x}, \dot{y}]^{\mathrm{T}}$, respectively. The position of the base station is $s = [x_i, y_i]^{\mathrm{T}}$. In this article, the superscript " $\cdot$ " notation is used to denote the corresponding rate of change, the right superscript "o" denotes the true value, and T denotes the transpose of the matrix. The actual distance between the target and the i_{th} base station is

$$r_i^o = \|s^o - p\| = \sqrt{(s^o - p)^{\mathrm{T}}(s^o - p)} \tag{17}$$

The TDOA measurement equation is

$$r_{i1}{}^o = r_i{}^o - r_1{}^o \tag{18}$$

Combining (17) with (18) and squaring them yields a specific set of TDOA equations, the expansion of which can be expressed as

$$r_{i1}^{o2} - s_i^{\mathrm{T}} s_i + s_1^{\mathrm{T}} s_1 = 2 r_{i1}^o r_1{}^o - 2(s_i - s_1) u^o \tag{19}$$

The time-difference equation can only estimate the position of the target, and for velocity estimation, it depends on the frequency-difference equation; taking the derivative of time in Equation (17) yields the relationship between the true distance change rate and the target position parameters, as

$$\dot{r}^o{}_i = \frac{(\dot{u}^o - \dot{s}_i)^{\mathrm{T}}(u - s_i)}{r_i{}^o} \tag{20}$$

The Doppler difference of the signal received by each base station and the reference base station can be written as

$$\mu_{i1}^o = \mu_i - \mu_1 = \frac{v_i f_0}{c} - \frac{v_1 f_0}{c} \tag{21}$$

To estimate the speed of the target, the FDOA equation can be obtained by taking the time derivative of (17), as

$$2(\dot{r}_{i1}^o r_{i1}^o + \dot{r}_{i1}^o r_i^o + r_{i1}^o \dot{r}_1^o) = 2(\dot{s}_i^{\mathrm{T}} - \dot{s}_1^{\mathrm{T}} s_1 - (\dot{s}_i - \dot{s}_1)^{\mathrm{T}} u^o - (s_i - s_1)^{\mathrm{T}} \dot{u}^o) \tag{22}$$

where $\dot{r}_{i1}^o$ represents the range different rate (RDR) for the variation in distance difference between the base stations. It can be found that TDOA and FDOA are closely related in the process of establishing the equations, and the relationship between them needs to be considered in order to realize the target localization and speed measurement.

Different from the ideal situation, in practical applications, when the base station receives the reflected signal for target positioning, it can only obtain the observed values of the time difference and frequency difference data, which contain measurement noise. The measured values of the distance difference vector and the distance difference rate of the change vector can be expressed as

$$\begin{cases} r = r^o + n_t \\ \dot{r} = \dot{r}^o + n_\mu \end{cases} \tag{23}$$

where n_t and n_μ are the measurement noise vectors of time and frequency differences, obeying the Gaussian distribution with zero mean and variance σ^2, and the covariance matrices are Q_t and Q_μ, respectively. The two measurements r and $\dot{r}$ are merged to form the localization parameter measurement vector $\beta = [r^{\mathrm{T}}, \dot{r}^{\mathrm{T}}]$, and the covariance matrix of the error vector between the true value and the measured value is $Q_\beta = E[\Delta\beta\Delta\beta^{\mathrm{T}}]$.

4.2. Weighted Least Squares Solutions

Least squares (LS) is a commonly used algorithm for solving localization problems, which essentially requires minimizing the sum of squares of estimation errors. The WLS assigns different weights to the observed values during the calculation process, essentially weighting the various items of the model to eliminate heteroscedasticity in the original mathematical model before parameter optimization. The positioning calculation process of WLS for TDOA/FDOA is as follows:

Firstly, define the variables to be measured $\theta^o = \left[u^{o\mathrm{T}}, r_1^o, \dot{u}^{o\mathrm{T}}, \dot{r}_1^o\right]^{\mathrm{T}}$, which include the unknown position of the target $u^{o\mathrm{T}}$, the velocity $\dot{u}^{o\mathrm{T}}$, the distance between the target and the reference base station r_1^o and the rate of change in the distance to the main base station $\dot{r}_1^o$. These four variables are uncorrelated. At this point, by replacing the observed values of (19) and (22) with the true values, the error vector of the positioning model obtained by combining them is

$$\lambda = h - G\theta \tag{24}$$

where

$$h = \begin{bmatrix} r_{21}^2 - s_2^{\mathrm{T}} s_2 + s_1^{\mathrm{T}} s_1 \\ r_{31}^2 - s_3^{\mathrm{T}} s_3 + s_1^{\mathrm{T}} s_1 \\ \vdots \\ 2(\dot{r}_{21} r_{21} - \dot{s}_2^{\mathrm{T}} s_2 + \dot{s}_1^{\mathrm{T}} s_1) \\ 2(\dot{r}_{31} r_{31} - \dot{s}_3^{\mathrm{T}} s_3 + \dot{s}_1^{\mathrm{T}} s_1) \end{bmatrix} \tag{25}$$

$$G = \begin{bmatrix} (s_2 - s_1)^{\mathrm{T}} & r_{21} & 0^{\mathrm{T}} & 0 \\ (s_3 - s_1)^{\mathrm{T}} & r_{31} & 0^{\mathrm{T}} & 0 \\ \vdots & \vdots & \vdots & \vdots \\ (\dot{s}_2 - \dot{s}_1)^{\mathrm{T}} & \dot{r}_{21} & (s_2 - s_1)^{\mathrm{T}} & r_{21} \\ (\dot{s}_3 - \dot{s}_1)^{\mathrm{T}} & \dot{r}_{31} & (s_3 - s_1)^{\mathrm{T}} & r_{31} \end{bmatrix} \tag{26}$$

where 0^{T} is a 1×3 row vector and the least squares estimate of θ^{o} is

$$\theta = \left[u^{\mathrm{T}}, r_1, \dot{u}^{\mathrm{T}}, \dot{r}_1\right]^{\mathrm{T}} = \left(G^{\mathrm{T}} W G\right)^{-1} G^{\mathrm{T}} W h \tag{27}$$

The weighting matrix in (27) is defined as follows:

$$W = B^{-\mathrm{T}} Q^{-1} B^{-1} \tag{28}$$

In the above equation, $B = \begin{bmatrix} B_t & O \\ B_\mu & B_t \end{bmatrix}$ and $B_t = 2diag\left\{r_2^o, r_3^o\right\}$ are the diagonal matrices of the distance between the base stations, $B_\mu = 2diag\left\{\dot{r}_2^0, \dot{r}_3^0\right\}$ is the diagonal matrix of the rate of change in the distance, and $Q = \begin{bmatrix} Q_t & O \\ O & Q_\mu \end{bmatrix}$ is the covariance matrix of the time–frequency difference data. Solve (27) to obtain the position and speed of the target; use the solution to update the weight matrix W, and substitute it into (27) again to complete the position estimation of the target.

5. Simulation Results and Performance Analysis

5.1. Performance Assessment Indicators

5.1.1. Root Mean Square Error

The performance of positioning and speed measurement can be evaluated and analyzed using root mean square error (RMSE), which is defined as

$$\mathrm{RMSE} = \sqrt{\frac{1}{\mathrm{n}}\sum_{i=1}^{m}\left(y_i - \hat{y}_i\right)^2} \tag{29}$$

The RMSE reflects the deviation between the estimated value and the true value of target speed measurement and positioning, which is easy to calculate and understand. The smaller the RMSE value, the more accurate the parameter estimation.

5.1.2. CRLB Performance Analysis

The CRLB is the lower bound of the unbiased estimator variance. To evaluate the radar performance of the integrated sensing algorithm proposed in this article, this section provides a performance analysis of CRLB. The true values of the position and speed of the HST to be located are given as $\theta^o = \left[u^{o\mathrm{T}}, r_1^o, \dot{u}^{o\mathrm{T}}, \dot{r}_1^o\right]^{\mathrm{T}}$, the true value of the base station position is given as p_{BS}^o, the total unknown vector is defined as $\phi^o\left[\theta^{o\mathrm{T}}, p_{BS}^{o\mathrm{T}}\right]^{\mathrm{T}}$, and the total observation vector is defined as $z = \left[\beta^{\mathrm{T}}, p_{BS}^{o\mathrm{T}}\right]^{\mathrm{T}}$. Firstly, calculate the joint probability density function (which has been taken as the natural logarithm) of the observation vector z under the given ϕ^o, as

$$\begin{aligned}&\ln f(z\left|\phi^o\right.) = \ln f(\beta\left|\theta^{o\mathrm{T}}, p_{BS}^o\right.) + \ln f(p_{BS}\left|\theta^{o\mathrm{T}}, p_{BS}^o\right.) = \\ &K - \tfrac{1}{2}[\beta - \beta^o]^{\mathrm{T}} Q_\beta^{-1}[\beta - \beta^o] - \tfrac{1}{2}[p_{BS} - p_{BS}^o]^{\mathrm{T}} Q_p^{-1}[p_{BS} - p_{BS}^o]\end{aligned} \tag{30}$$

Then, derive the Fisher Information Matrix (FIM) as follows:

$$\mathrm{FIM}(\phi) = -\mathrm{E}\left(\frac{\partial \ln^2 p(z\left|\phi^o\right.)}{\partial\phi^o\partial\phi^{o\mathrm{T}}}\right) = \mathrm{E}\left[\left(\frac{\partial \ln p(z|\phi^o)}{\partial\phi^o}\right)\left(\frac{\partial \ln p(z|\phi^o)}{\partial\phi^o}\right)^{\mathrm{T}}\right] \tag{31}$$

Based on the relationship that the CRLB is the reciprocal of the FIM, the CRLB of the parameter ϕ^o to be estimated can be obtained, as

$$\mathrm{CRLB}(\phi^o) = [FIM(\phi^o)]^{-1} = \begin{bmatrix} X & Y \\ Y^{\mathrm{T}} & Z \end{bmatrix}^{-1} \tag{32}$$

where X, Y, Z, respectively, denote

$$\begin{cases} X = \left(\frac{\partial\beta^o}{\partial\theta^{o\mathrm{T}}}\right)^{\mathrm{T}} Q_\beta^{-1}\left(\frac{\partial\beta^o}{\partial\theta^{o\mathrm{T}}}\right) \\ Y = \left(\frac{\partial\beta^o}{\partial\theta^{o\mathrm{T}}}\right)^{\mathrm{T}} Q_\beta^{-1}\left(\frac{\partial\beta^o}{\partial p_{BS}^{o\mathrm{T}}}\right) \\ Z = \left(\frac{\partial\beta^o}{\partial p_{BS}^{o\mathrm{T}}}\right)^{\mathrm{T}} Q_\beta^{-1}\left(\frac{\partial\beta^o}{\partial p_{BS}^{o\mathrm{T}}}\right) + Q_p^{-1} \end{cases} \tag{33}$$

where Q_β and Q_p represent the covariance matrices of the error vectors between the true and measured values about β and p_{BS}, respectively. In practical applications, the main focus is on the position and velocity parameters of the target θ^o, and the corresponding matrix $\mathrm{CRLB}(\theta^o)$ represents the 6×6 sub-matrix on the upper left of $\mathrm{CRLB}(\phi)$, so the CRLB of θ^o can be expressed as

$$\mathrm{CRLB}(\theta^o) = \left(X - YZ^{-1}Y^{\mathrm{T}}\right)^{-1} \tag{34}$$

The horizontal axis in Figure 4 represents the power of noise, expressed in logarithmic form and measured in dB. The vertical axis represents the RMSE of position or velocity estimation, measured in meters or m/s. From Figures 4 and 5, it can be seen that the accuracy of position estimation is higher than that of velocity estimation. When the measurement noise is below 4 dB, the RMSE for target localization can match the CRLB. However, as the noise level continues to increase, the position error also increases significantly. The RMSE for target speed measurement can reach CRLB when the measurement noise is below 0 dB. As the noise level continues to increase, the speed measurement error also increases significantly.

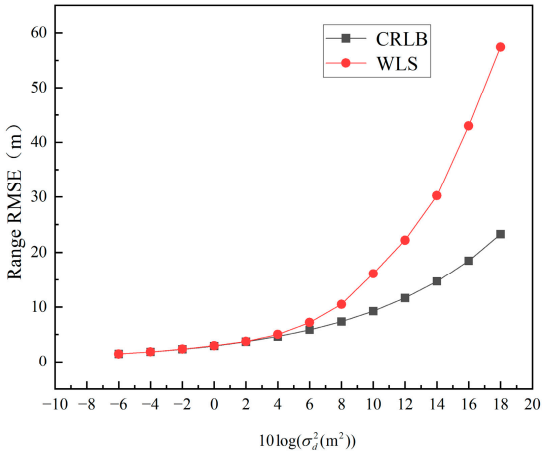


Figure 4. Comparison between RMSE of position estimation and CRLB.

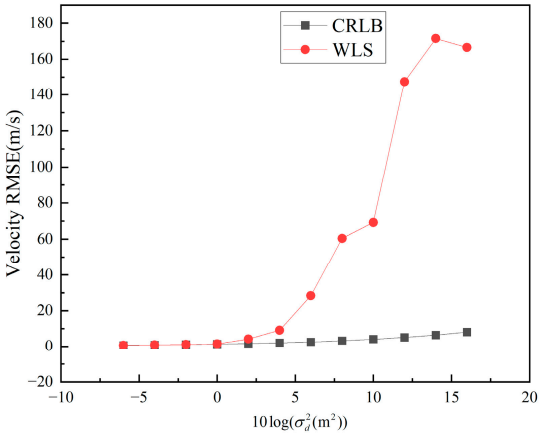


Figure 5. Comparison between RMSE of velocity estimation and CRLB.

5.2. Radar Performance Analysis

In order to verify the effectiveness of the proposed scheme, this section will simulate and validate the radar communication integrated signal based on OTFS and compare the algorithm proposed in this article with the multiple signal classification (MUSIC) algorithm and the CCC algorithm [8]. The simulation parameters are shown in Table 1. Table 2 shows the actual position coordinates of the three base stations and Table 3 shows the estimated position and velocity of the targets. Under the experimental parameters set in the following three tables, the simulation platform of this experiment is Matlab 2023a. The running environment is Intel(R) Core (TM) i7-13700F (2.1GHz), NVIDIA RTX4070Ti.

Table 1. Simulation parameters.

Parameters	Value	Parameters	Value
Carrier frequency/GHz	3	Base station pacing/m	500
Symbolic average energy	1	Number of iterations	100
Number of subcarriers	64	Radar SNR/dB	5
Subcarrier spacing	32	Cyclic prefix length	128
HSR speed/(m/s)	0–139	Distance/m	30

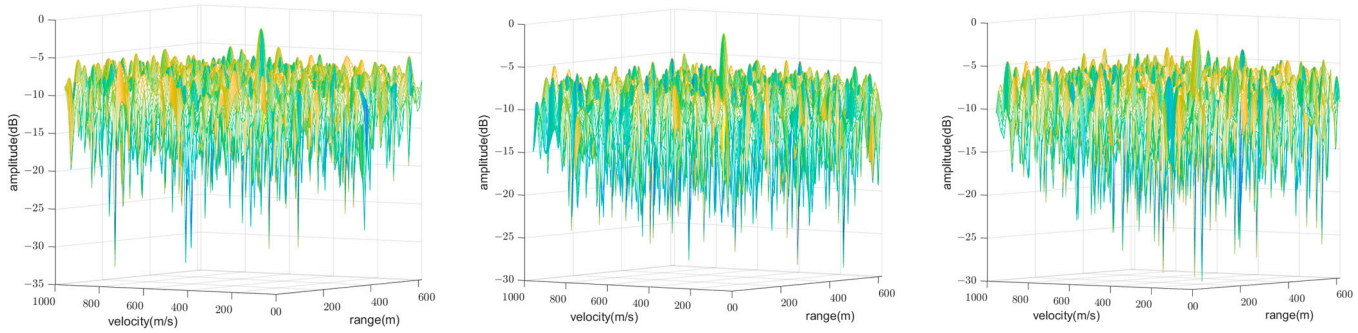
Table 2. True position of the base stations.

Name	x_i/m	y_i/m
Base station 1	0	0
Base station 2	2000	40
Base station 3	4000	60

Table 3. Estimated position and velocity of the target.

Number	r_i/m	$\hat{r}_i$/m	v_i/m/s	$\hat{v}_i$/m/s
1	30	29.98	97.22	97.86
2	40	39.98	111.11	110.92
3	100	100.16	138.89	139.53

Figure 6 shows the echograms of the radar signals received by the three base stations at an SNR of 10 dB. The x and y coordinates of the spike position correspond to the speed and distance of the target, respectively, and the z-axis represents the amplitude of the radar signals, with the spike position z = 0 dB. Usually, closer targets or higher-power radar systems produce stronger echo signals, which are manifested by higher spike amplitudes. By using the parameter estimation algorithm in Section 3 to process radar signal echoes, the time delay and Doppler information of the target can be obtained. Based on the arrival time difference and Doppler information obtained from each base station, the positioning and velocity estimation algorithm proposed in Sections 4.1 and 4.2 is used to estimate the position and velocity of the target.



(**a**) Base Station 1 (**b**) Base Station 2 (**c**) Base Station 3

Figure 6. Radar signal echo diagram.

We compare the MUSIC algorithm and CCC algorithm with the algorithm proposed in this article when the SNR varies from 0 dB to 10 dB under the condition of an HST movement speed of 139 m/s. The RMSE is used to measure the radar detection performance and is represented by the vertical axis. The simulation comparison results are shown in Figure 7. Under the same SNR of 10 dB, the speed estimation of the perception algorithm in this article can achieve an accuracy of decimeters per second, which has significant advantages compared to the other two algorithms.

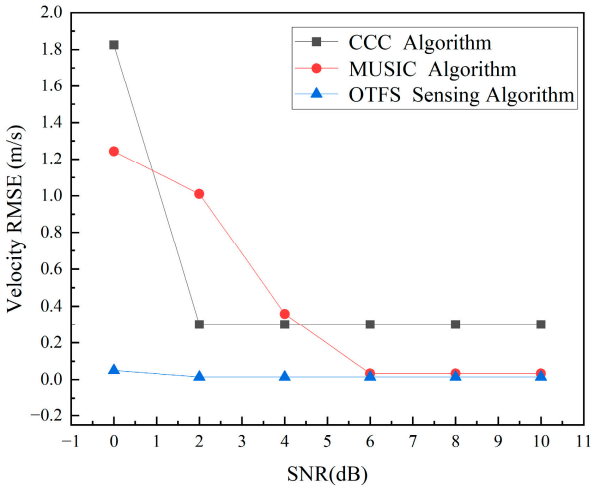


Figure 7. Velocity tracking error of algorithms under different SNR conditions.

Figure 8 shows the RMSE of distance estimation for each algorithm under different SNR conditions. It can be observed that the three algorithms are less affected by noise, but the two-stage estimation algorithm used in this article achieves millimeter-level distance estimation accuracy with an SNR of 10 dB.

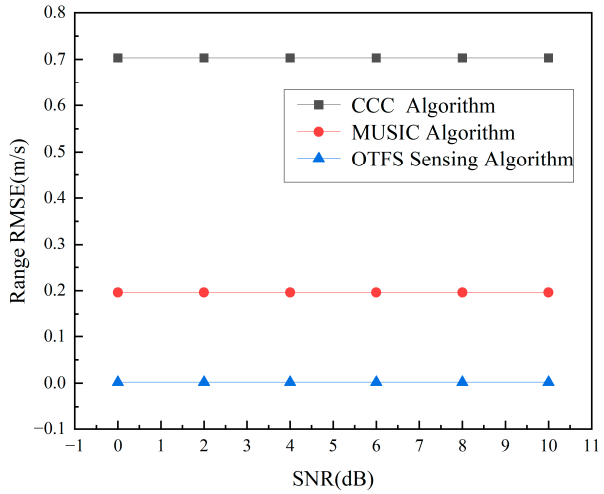


Figure 8. Distance estimation error of algorithms under different SNR conditions.

Next, the proposed algorithm is compared with the widely used GNSS/INS combined positioning and speed measurement algorithm in train positioning. The data fusion part of GNSS/INS uses EKF. The two algorithms are compared in the scenario where the train runs at a speed of 0–139 m/s. As shown in Figure 9, in the stationary state of the train, the measurement error of both positioning methods for train speed is 0, and with the increase in speed, the RMSE of GNSS/INS for speed increases from 0 to 7.71. The RMSE of the OTFS-ISAC perception algorithm in this article is maintained around 1, with lower estimation bias and significant advantages compared to GNSS/INS.

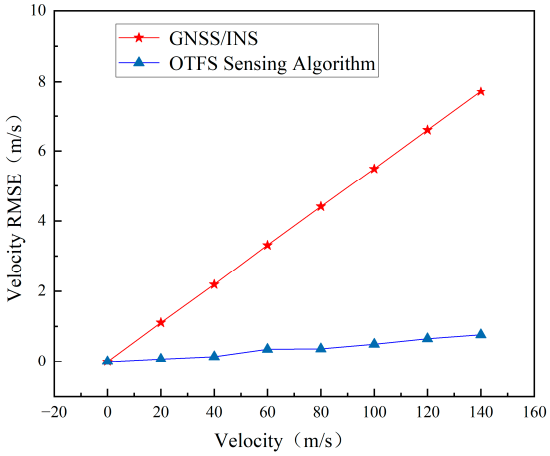


Figure 9. Comparison of proposed algorithms with GNSS/INS at different speeds.

5.3. Complexity and Time Performance Analysis

This section briefly analyzes the complexity and time performance analysis of the proposed TSE algorithm. The algorithm realizes the super-resolution estimation of the sensing target parameters. The estimation result can be a non-integer multiple of the system delay and Doppler resolution. The proposed TSE algorithm helps to reduce the complexity of the system, because it excludes the dictionary matrix that needs a lot of calculation in the second step of refined search. The specific operation is to re-establish a new smaller area Λ_i to conduct off-grid search after the first stage of rough estimation, thus greatly reducing the search interval and ultimately reducing the complexity of the algorithm. At the same time, the algorithm is conducted in the time domain, so it does not need to convert to the time-delay Doppler domain for parameter estimation. The complexity of the TSE algorithm in this article is $O(MN\log(MN))$.

In addition, this article compared the time of the proposed algorithm with the CCC algorithm [8] and two-dimensional fast Fourier transform (2D-FFT) algorithm in a single run, and recorded the running time of each algorithm five times in a row. It can be seen that the running time of the proposed TSE algorithm is relatively short. The comparison results are shown in Table 4.

Table 4. Comparison of running times of different algorithms.

Parameter Estimation Algorithm	Running Time (Unit: Second)				
TSE algorithm	0.234	0.221	0.202	0.210	0.212
CCC algorithm [8]	0.764	0.721	0.795	0.807	0.744
2D-FFT algorithm	0.537	0.587	0.609	0.629	0.688

6. Conclusions

Based on the modulation principle of OTFS and the characteristics of signal processing in the DD domain, OTFS is integrated with communication perception technology and applied in HST speed measurement and positioning scenarios. This article proposes an OTFS-based integrated sensing positioning and speed measurement algorithm for HST scenarios. Firstly, the composition structure of the radar communication integrated system based on OTFS modulation is analyzed, and the system scenario is analyzed. System parameters that meet the performance indicators of the radar and communication system were designed, and the TSE algorithm was used to estimate the speed and distance parameters of the HST. Then, the train is located and measured using TDOA/FDOA, and the CRLB for positioning and speed measurement of this method is derived. The comparative experimental results show that the algorithm proposed in this article has better positioning and speed measurement performance compared to OFDM radar and GNSS/INS combined positioning algorithms.

In terms of radar operating mode, this article only uses the simpler monostatic radar scheme. Therefore, the next step of work will consider expanding to the bistatic radar system to adapt to complex HST positioning and speed measurement scenarios with higher detection range and accuracy. In future research, the OTFS-based communication perception integrated positioning and speed measurement algorithm will play an important role in HST autonomous driving, natural disaster monitoring, and improving the safe transportation capacity of HST.

Author Contributions: Conceptualization, J.X., Y.H., C.L. and H.W.; methodology, J.X., Y.H., C.L. and H.W.; validation, J.X. and Y.H.; writing—original draft preparation, Y.H.; writing—review and editing, J.X. and Y.H.; supervision, J.X. and C.L. All authors have read and agreed to the published version of the manuscript.

Funding: This research was funded by the National Natural Science Foundation of China (62161016).

Data Availability Statement: Data are contained within the article.

Conflicts of Interest: The authors declare no conflicts of interest. The funders had no role in the design of the study; in the collection, analyses, or interpretation of data; in the writing of the manuscript; or in the decision to publish the results.

References

1. Mo, Z.; An, H. Research on Comprehensive Autonomous Positioning Technology of New Train Control System. *J. China Railw. Soc.* **2022**, *44*, 56–64.
2. Liu, D.; Jiang, W.; Cai, B. Train Localization Method for Tightly-coupled GNSS/INS Integrated Strategy Based on Simplified Robust UKF. *J. China Railw. Soc.* **2023**, *45*, 62–71.
3. Wang, Z.; Wang, Y.; Li, W. Research on BDS Information Fusion Algorithm of JingZhang High Speed Intelligent EMU. *J. Dalian Jiaotong Univ.* **2023**, *44*, 101–106.
4. Wang, Z.; Yu, G.; Zhou, B.; Wang, P.; Wu, X. A train positioning method based-on vision and millimeter-wave radar data fusion. *IEEE Trans. Intell. Transp. Syst.* **2021**, *23*, 4603–4613. [CrossRef]
5. Zhu, L.; He, D.; Zhong, Z. Application of Radar Communication Integration in Intelligent Railway. *China Railw.* **2021**, *1*, 17–24.
6. Wen, J.; Yi, X.; Han, K.; Chen, L. A New Paradigm of High-Precision Localization: Integrated Communication and Localization Technology and Application. *Mob. Commun.* **2023**, *47*, 17–25+109.
7. Liu, F.; Yuan, W.; Masouros, C.; Yuan, J. Radar-assisted predictive beamforming for vehicular links: Communication served by sensing. *IEEE Trans. Wirel. Commun.* **2020**, *19*, 7704–7719. [CrossRef]
8. Wu, K.; Zhang, J.A.; Huang, X.; Guo, Y.J. Integrating low-complexity and flexible sensing into communication systems. *IEEE J. Sel. Areas Commun.* **2022**, *40*, 1873–1889. [CrossRef]
9. Zhou, B.; Ma, S. Simultaneous vehicular location and velocity detection towards 6G integrated communication and sensing. *J. Commun.* **2023**, *44*, 81–92.
10. Zhang, K.; Yuan, W.; Li, S.; Liu, F.; Gao, F.; Fan, P.; Cai, Y. Radar sensing via otfs signaling: A delay doppler signal processing perspective. In Proceedings of the ICC 2023-IEEE International Conference on Communications, Rome, Italy, 28 May–1 June 2023; pp. 6429–6434.
11. Yuan, W.; Wei, Z.; Li, S.; Yuan, J.; Ng, D.W.K. Integrated sensing and communication-assisted orthogonal time frequency space transmission for vehicular networks. *IEEE J. Sel. Top. Signal Process.* **2021**, *15*, 1515–1528. [CrossRef]
12. Wei, Z.; Li, S.; Yuan, W.; Schober, R.; Caire, G. Orthogonal time frequency space modulation—Part I: Fundamentals and challenges ahead. *IEEE Commun. Lett.* **2022**, *27*, 4–8. [CrossRef]
13. Bondre, A.S.; Richmond, C.D. Dual-use of OTFS architecture for pulse Doppler radar processing. In Proceedings of the 2022 IEEE Radar Conference (RadarConf22), New York, NY, USA, 21–25 March 2022; pp. 1–6.
14. Wang, X.; Xiaogang, T.; Yiqing, Z.; Chong, Z.; Zhengang, P. Survey of channel estimation method in delay-Doppler domain for OTFS. *J. Commun.* **2022**, *43*, 188–201.
15. Gaudio, L.; Kobayashi, M.; Caire, G.; Colavolpe, G. On the effectiveness of OTFS for joint radar parameter estimation and communication. *IEEE Trans. Wirel. Commun.* **2020**, *19*, 5951–5965. [CrossRef]
16. Dehkordi, S.K.; Gaudio, L.; Kobayashi, M.; Caire, G.; Colavolpe, G. Beam-space MIMO radar for joint communication and sensing with OTFS modulation. *IEEE Trans. Wirel. Commun.* **2023**, *22*, 6737–6749. [CrossRef]
17. Liu, R.Y.; Liu, R.; Li, J.; Pan, Z. Three-Dimensional Joint Localization for Integrated Sensing and Communication Systems. *Mob. Commun.* **2024**, *48*, 90–94.
18. Wang, J.; Ma, H.; Liang, X.; Li, Y.; Chen, L. Research on Integrated Radar Communication Technology Based on Delay-Doppler Modulation. *J. Signal Process.* **2023**, *39*, 1047–1059.
19. Sun, C.; Li, L.; ZHANG, H. OTFS-enabled integrated sensing and communication techniques for next-generation V2X networks. *Chin. J. Eng.* **2023**, *45*, 1674–1683.

20. Wu, Y.; Jia, H.; Nakawaki, Y.; Pan, Z.; Shimamoto, S. Doppler-Only Wireless Positioning for High-Speed Railway Based on Fractional Doppler Estimation. In Proceedings of the 2024 IEEE Wireless Communications and Networking Conference (WCNC), Dubai, United Arab Emirates, 21–24 April 2024; pp. 1–6.
21. Zhao, S.; Du, H.; Liu, Z.; Yu, J. OTFS Radar Communication Integrated Multiplexed Waveform Design. *J. Signal Process.* **2024**, *40*, 1239–1248.
22. Raviteja, P.; Phan, K.T.; Hong, Y. Embedded pilot-aided channel estimation for OTFS in delay–Doppler channels. *IEEE Trans. Veh. Technol.* **2019**, *68*, 4906–4917. [CrossRef]
23. Xiong, L.; Liu, X.; Gong, J.; Peng, M. Orthogonal Time Frequency Space Modulation-based Sensing Signal Processing Algorithms. *Radio Commun. Technol.* **2023**, *49*, 100–109.
24. Wu, Y.; Han, C.; Chen, Z. DFT-spread orthogonal time frequency space system with superimposed pilots for terahertz integrated sensing and communication. *IEEE Trans. Wirel. Commun.* **2023**, *22*, 7361–7376. [CrossRef]
25. Du, Z.; Liu, F.; Yuan, W.; Masouros, C.; Zhang, Z.; Xia, S.; Caire, G. Integrated sensing and communications for V2I networks: Dynamic predictive beamforming for extended vehicle targets. *IEEE Trans. Wirel. Commun.* **2022**, *22*, 3612–3627. [CrossRef]

Disclaimer/Publisher's Note: The statements, opinions and data contained in all publications are solely those of the individual author(s) and contributor(s) and not of MDPI and/or the editor(s). MDPI and/or the editor(s) disclaim responsibility for any injury to people or property resulting from any ideas, methods, instructions or products referred to in the content.